Korean J. Chem. Eng., 34(3), 892-897 (2017)
DOI: 10.1007/s11814-016-0303-3

pISSN: 0256-1115
eISSN: 1975-7220

Organic/inorganic multilayer thin film encapsulation via initiated chemical vapor deposition and atomic layer deposition for its application to organic solar cells

Bong Jun Kim*, Donggeon Han, Seunghyup Yoo**, and Sung Gap Im*,†**

*Department of Chemical & Biomolecular Engineering, Korea Advanced Institute of Science and Technology, Daejeon 34141, Korea
**Department of Electrical Engineering, Korea Advanced Institute of Science and Technology, Daejeon 34141, Korea
(*Received 13 August 2016 • accepted 24 October 2016*)

Abstract−A thin film encapsulation (TFE) was fabricated by alternating deposition of organic and inorganic layers via initiated chemical vapor deposition (iCVD) and atomic layer deposition (ALD). A highly crosslinked organosilicone polymer, poly(1,3,5-trimethyl-1,3,5-trivinylcyclotrisiloxane) (pV3D3) was successfully adopted as the organic layer for the fabrication of TFE. The film formed a stable and smooth interface with ALD Al_2O_3 layer. The multilayer TFE consisting of pV3D3 and Al_2O_3 alternating layers exhibited outstanding optical transparency as well as excellent barrier property. Finally, the multilayer TFE was applied monolithically to organic solar cells (OSCs), and the shelf life of the cells was increased immensely, suggesting that the developed organic/inorganic multilayer TFE is an efficient barrier film for elongating the lifetime of organic electronics.

Keywords: Initiated Chemical Vapor Deposition (iCVD), Atomic Layer Deposition (ALD), Thin Film Encapsulation (TFE), Barrier, Organic Solar Cells (OSCs)

INTRODUCTION

The fossil fuel-based energy crisis has focused continuous attention on developing clean and renewable energy. The most highlighted alternative energy is solar energy due to its cleanness and the sustainability. Organic solar cells (OSCs) have made impressive development in last two decades owing to their advantageous characteristics such as light-weight, flexibility, and low fabrication cost [1-3]. However, low efficiency, has been one of the major challenges for OSCs. Thus, there have been numerous research efforts to resolve this issue, which have resulted in a substantially increased power conversion efficiency (PCE) of up to 11% for single junction cells [4], and 12% for tandem junction cells [5].

However, the insufficient stability of OSCs still hinders the industrial application of the devices [6]. Diverse origins had been suggested to explain the instability of OSCs, including the metastable morphology of the cell, diffusion of electrodes and buffer layers, the instability upon irradiation or exposure to heat during the operation [7]. Among them, the high reactivity of the photoactive materials in OSCs with oxygen and water vapor is the major factor that limits the stability of the cells. As oxygen and water vapor are penetrating into the OSCs, they can oxidize various parts of the cells - electrodes, active layer, and buffer layers - to deteriorate device performance [8]. To overcome this issue, various strategies had been attempted. New material design of the active layer could enhance the stability of the device against oxidation by replacing oxidizable units in the active layer with more stable functionalities [9,10]. Applying inverted geometry also reportedly increased the cell stability as the trap-mediated recombination could be inhibited [11]. Introducing an oxide buffer layer such as MoO_x on top of the active and electron-transporting layer (ETL) also effectively blocked the penetration of oxygen and water vapors [12]. Optimizing buffer layers [13,14], as well as using air-stable electrode materials such as noble metal-based nanowire, graphene, and modified indium tin oxide (ITO) could contribute to increase in OSC stabilities [15,16].

Applying an encapsulation layer is an indispensable method to enhance the stability of the device, since this approach simply prevents the cells from contacting oxygen and water vapor during operation [8]. It has been widely acknowledged that a water vapor transmission rate (WVTR) below 10^{-4} g·m^{-2}·day^{-1} is required to satisfy the encapsulation demand of OSCs [17]. In previous studies, we have reported that an effective thin film encapsulation (TFE) can be fabricated by alternative deposition of organic and inorganic layers via initiated chemical vapor deposition (iCVD) and atomic layer deposition (ALD), respectively [18,19]. ALD can provide a highly dense inorganic film with outstanding barrier property at relatively low temperature, less than 100 °C [20], while iCVD can provide a pinhole-free, conformal organic layer, which enables the formation of an excellent interface with inorganic layers [21-23].

We developed a new organic material, poly(1,3,5-trimethyl-1,3,5-trivinylcyclotrisiloxane) (pV3D3) as the organic layer for the fabrication of high-performance TFE, when coupled with ALD processed Al_2O_3 inorganic layer. The TFE film made of iCVD pV3D3/ALD Al_2O_3 multilayers exhibited outstanding optical and barrier properties that make the TFE a strong candidate barrier film for organic electronic devices. The developed multilayer TFE was applied directly onto OSC as shown in Fig. 1 to demonstrate the capability of the TFE to elongate the lifetime of organic electronic devices. A three dyad-multilayer TFE was integrated monolithically to OSCs, which could successfully block the penetration of oxygen and water

†To whom correspondence should be addressed.
E-mail: sgim@kaist.ac.kr

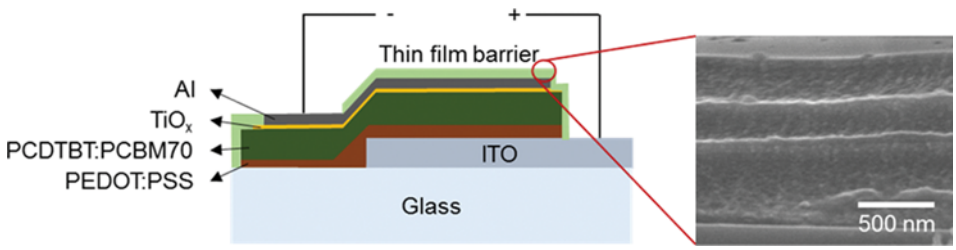

Fig. 1. Schematic of an OSC encapsulated with iCVD/ALD multilayer TFE. The corresponding cross-sectional SEM image is shown on the right.

vapor under an accelerated condition (27 °C, 90% relative humidity (RH)), thereby increasing the shelf life of the OSCs immensely. This study clearly confirms that the iCVD/ALD multilayer TFE with the superior barrier property can play a critical role in achieving a stable, long-term operation of OSCs.

EXPERIMENTAL

1. Film Depositions

pV3D3 was deposited via iCVD process, whose procedure was reported in detail elsewhere [24]. The monomer of pV3D3, 1,3,5-trimethyl-1,3,5-trivinylcyclotrisiloxane (V3D3, Gelest, 95%) and the initiator, *tert*-butyl peroxide (TBPO, Aldrich, 98%) were vaporized into an iCVD reactor (Daeki Hi-Tech) with the flow rates of 2.5 and 1 sccm, respectively. To achieve the desired flow rate, V3D3 was heated to 40 °C while TBPO was sufficiently volatile not to require additional heating. All the chemicals were used as purchased without further purification. During the deposition, the filament was heated to 140 °C, the substrate temperature was maintained at 40 °C, and the chamber pressure was set to 300 mTorr.

Al_2O_3 film was deposited by ALD system (LUCIDA D100, NCD). The chamber temperature was maintained at 90 °C to minimize the thermal damage on OSCs during the process. The sequence of ALD cycle consisted of a 0.2 s trimethyl aluminum (TMA, UP Chemical Co. Ltd.) injection, 10 s purging with N_2, 0.2 s deionized (DI) H_2O injection, and 10 s purging with N_2.

2. Film Property Measurements

The surface morphology and the roughness were assessed with atomic force microscopy (AFM, XE-100, Park Systems) at a non-contact AFM mode. The transmittance of the layers was analyzed by ultraviolet-visible spectroscopy (UV-Vis, Shimadzu UV-3600). The cross-sectional image of the multilayer was obtained with a scanning electron microscope (SEM, Hitachi S4800). The density was measured by X-ray reflectometry (XRR, RIGAKU, SmartLab), and the refractive index was obtained by spectroscopic ellipsometer (M2000D, J.A. Woollam, Lincoln).

The barrier property was measured via optical calcium test. Using a thermal evaporator (Daeki Hi-Tech Co. Ltd.) in a N_2-filled glove box, 50 nm-thick Ca (99.5%, Junsei Chemical) film was deposited on a 1 mm-thick glass substrate. On a glass substrate with the area of 25 mm×25 mm, four separate Ca layers with the area of 3 mm×3 mm were deposited at a constant deposition rate around 1.0 Å s^{-1}. Organic/inorganic multilayers were deposited onto the Ca layer via iCVD and ALD processes. After the multilayer fabrication on Ca layer, the encapsulated samples were placed in a thermo-hygrostat (TM-EM-065, JEIO Tech) set to 27 °C and 90% RH. A digital camera (Nikon P300) was used to take images of the samples at a preset time. Then the obtained images were processed by Image J (National Institutes of Health) to calculate the oxidized area of Ca for each sample. From the calculated data, a plot showing the rate of change of Ca-oxidized area could be obtained. After that, the water vapor deposition rate (WVTR) could be calculated from Eq. (1) [25].

$$\mathrm{WVTR}[\mathrm{g\cdot m^{-2}\cdot day^{-1}}] = \mathrm{n}\cdot\delta_{Ca}\frac{\mathrm{M(H_2O)}}{\mathrm{M(Ca)}}\cdot\mathrm{h}\cdot\frac{\mathrm{dA}}{\mathrm{dt}} \quad (1)$$

where n is the molar equivalent of the Ca with water molecule during CaO_2 formation (n=2), δ_{Ca} is the Ca density (1.55 g·cm^{-3}). $M(H_2O)$ and M(Ca) are the molecular weights of water and Ca, respectively; h is height of the Ca film, and dA/dt is slope of the plotted graph showing the rate of change of Ca-oxidized area.

3. OSC Shelf Life Measurement

Glass substrates with ITO-pattern were used for the device fabrication. The substrates were sequentially cleaned with soapy water, DI water, acetone, and isopropanol in an ultrasonic bath. The ITO surface was treated with oxygen plasma to reduce contaminants before layer depositions. The OSCs were fabricated following the structure: 30 nm of poly(3,4-ethylenedioxythiophene) : poly(styrenesulfonate) (PEDOT : PSS)/60 nm of a blend of poly[N-9″-heptadecanyl-2,7-carbazole-alt-5,5-(4′,7′-di-2-thienyl-2′,1′,3′-benzothiadiazole)] (PCDTBT) (1-Material, Inc.) and [6,6]-phenyl C_{70}-butyric acid methyl ester (PCBM70) (Nano-C, Inc.)/5 nm of TiO_x/100 nm of Al. All the materials were spin coated except for Al, which was deposited via thermal evaporator. The coating procedure for PCDTBT : PCBM70 and TiO_x is described in detail in a previous work [12].

After depositing various structures of barrier films on the devices, they were placed in a thermo-hygrostat (TH-PE-025, JEIO Tech). The chamber was set with an accelerated condition of 27 °C and 90% RH, which is identical to the Ca test condition and close to ISOS-D-3 [26]. After a pre-set time, the devices were taken out of the thermos-hygrostat for current density-voltage (*J-V*) characterization, and then were placed back in. The *J-V* characteristics were measured with a source-measure unit (Keithley 238) under AM 1.5G illumination from a solar simulator (ABET Technologies). The irradiance of the light source was checked periodically using a calibrated Si photodiode. For each dyad of the multilayer, five cells were measured and the best data was collected to minimize underestimation of the shelf life due to extrinsic factors such as side penetration or particle contamination during device fabrication and encapsulation.

RESULTS AND DISCUSSION

Al_2O_3 layer was selected as the inorganic layer for the TFE fabrication due to its outstanding barrier property [27]. Al_2O_3 film applied in this study had a growth rate of 1.14 Å/cycle as shown in Fig. S1(a), which indicates that the deposition was successfully conducted in ALD mode. The refractive index, n of the film was 1.61 and the density was 2.97 g/cm^3. In this work, pV3D3 layer was newly introduced as the organic layer of the TFE. It was previously presented that the pV3D3 layer via iCVD process is highly smooth, flexible with exceptionally high density - about 1.71 g/cm^3 - for plastics [28]. Those properties are suitable not only for dielectric layer application, but also for TFE application. The smooth surface of the film is highly desirable to form an intact interface with following inorganic layers with minimal defect density. The low roughness is also critically important to minimize the pinhole formation, which is, in turn, necessary to warrant the higher barrier performance [29]. The mechanical robustness of the organic layer is another significant factor to be considered, since the flexibility of TFE is often closely related to mechanical property of the organic materials [30]. Our previous observation indicates that pV3D3 maintained its insulating property even at 4% of applied strain, demonstrating its excellent mechanical flexibility [28]. The high density of the pV3D3 organic layers will also be advantageous for forming high-performance TFE by elongating the tortuous path of the penetrating vapors, thereby effectively decreasing the WVTR value of the TFE [31]. These characteristics of pV3D3 observed in the previous work are all ideal for TFE application.

For the TFE application of pV3D3 layer, it is important to secure a smooth interface with Al_2O_3 layer deposited via ALD. Especially, on top of relatively soft organic layer, the deposition of hard inorganic layer can cause unwanted interfacial damages such as cracks, pinholes, and wrinkles due to the surface energy difference and the build-up of interfacial stress between the organic/inorganic layers. To investigate the interfacial stability of the hybrid layer, 25 nm of Al_2O_3 was deposited on 100 nm-thick pV3D3 layer, and the surface morphology was examined by AFM (Fig. 2). The hybrid multilayer surface maintained its smooth nature with extremely low root mean square (RMS) roughness of 0.316 nm without any apparent damage of the inorganic layer surface, confirming the formation of stable interface between the iCVD pV3D3 with ALD Al_2O_3. As a negative control, ALD Al_2O_3 was deposited on uncrosslinked, linear acrylate polymers such as poly(cyclohexyl methacrylate) (pCHMA) and poly(hydroxyethyl methacrylate) (pHEMA) and the surfaces of Al_2O_3 were investigated analogously by AFM. Unlike the surface of Al_2O_3 on pV3D3 layer, pinhole induced by dewetting, and wrinkle formation were clearly observed on pCHMA and pHEMA, respectively, as shown in Fig. 2(c) and 2(d). The observation is because the uncrosslinked polymer chain becomes mobile during the Al_2O_3 deposition at an increased deposition temperature at 90 °C, which causes the interfacial instability. On the other hand, the highly crosslinked pV3D3 layer is thermally stable and resistant to the chain movement. In addition, due to the exceptionally high density of the pV3D3 layer, the polymer surface maintained its smooth surface at high temperature during the Al_2O_3 deposition [28]. This observation confirms that the highly crosslinked, densely packed pV3D3 is suitable for the formation of a stable interface with the ALD Al_2O_3 layer, and consequently the fabrication of organic/inorganic multilayer TFE.

Fig. 3 illustrates the light transmittance of the pV3D3, Al_2O_3 and pV3D3/Al_2O_3 multilayer. The average transmittances of both 300 nm-thick pV3D3 layer and 25-nm thick Al_2O_3 layer in the visible light region (380-800 nm) were higher than 99%. Even after stacking the two films to form one dyad-multilayer TFE, such a high transparency was preserved. The organic/inorganic multilayer composed of 300 nm-thick pV3D3 and 25 nm-thick Al_2O_3 showed average transmittance of 99.5% with no apparent transparency fluctuation throughout the visible light region. These exceptionally high transmittance values are advantageous for optoelectronic devices in that the decrease of incident light intensity by the additional TFE can be minimized.

Our previous investigation on the TFE structure indicated that

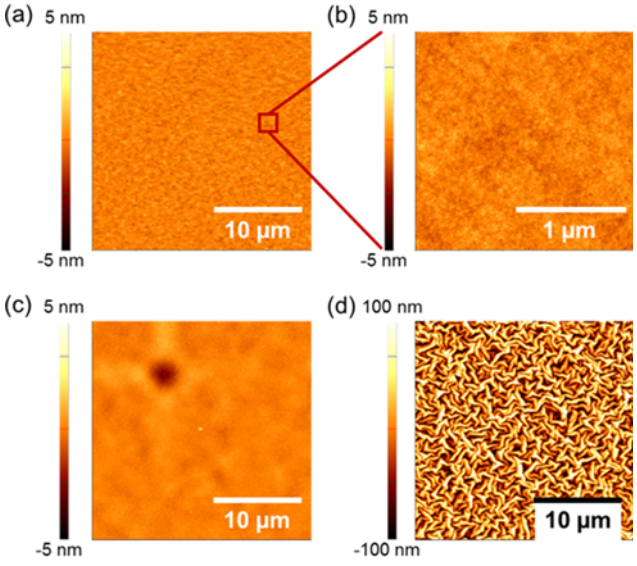

Fig. 2. AFM surface morphologies of films of 25 nm-thick Al_2O_3 on pV3D3 with the size of (a) 25×25 μm^2 and (b) 2×2 μm^2. Surface deformation observed via AFM after deposition of 25 nm-thick Al_2O_3 on (c) pCHMA and (d) pHEMA.

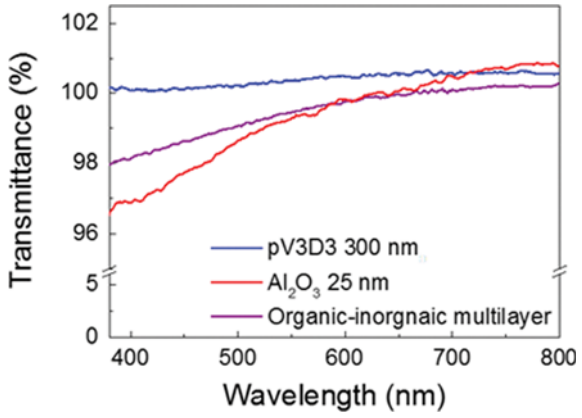

Fig. 3. Transmittance of 300 nm-thick pV3D3, 25-nm thick Al_2O_3 layer, and one dyad of the pV3D3/Al_2O_3 multilayer.

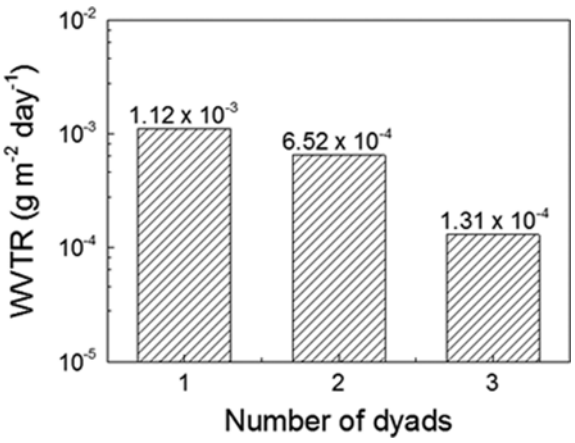

Fig. 4. WVTR of the multilayer TFE with one to three dyads of alternating pV3D3/Al_2O_3 layers.

the first organic layer should be thick enough to conformally cover the active layer underneath with the smooth, pinhole-free organic layer [18]. The thick first layer is also required to serve as an efficient temporary barrier before and during ALD process since the ALD process includes a pulse of H_2O input during the deposition, which must be blocked in order not to damage the active layer underneath. On the other hand, the thickness of other organic layers beyond first dyad could be reduced to shorten the fabrication time. Analogously, the pV3D3/Al_2O_3 multilayer TFE was fabricated according to the optimized structure suggested previously. 500 nm-thick pV3D3 layer was sufficient to function as the initial barrier for TFE fabrication. The structure of three dyads of the multilayer was illustrated in the SEM image of Fig. 1. The interface of the multilayers was intact even after 100 times of tape test and 90 minutes of exposure to ultrasonication. The barrier performance of the multilayer TFE with one to three dyads of organic/inorganic multilayer was monitored via Ca test. As expected, increasing the number of dyads resulted in the increase of barrier property. One dyad-multilayer TFE exhibited a WVTR value as low as 1.12×10^{-3} g·m^{-2}·day^{-1}, while the WVTR of three dyad-multilayer TFE was 1.31×10^{-4} g·m^{-2}·day^{-1}, which is nearly ten times lower than that of the one dyad-multilayer TFE. In comparison, one dyad-multilayer TFE with 100 nm-thick Al_2O_3 film had WVTR of 2.16×10^{-4} g·m^{-2}·day^{-1}. Although the three-dyad multilayer TFE consisted of thinner total thickness of inorganic layers, it showed better barrier performance since the tortuous path of penetrating vapors were increased due to insertion of the iCVD organic layers in between the inorganic layers. These WVTR values were obtained in an accelerated condition of 27 °C and 90% RH. Considering the acceleration factor proposed by Coyle [32], the WVTR value of the three dyad-multilayer corresponds to 1.27×10^{-5} g·m^{-2}·day^{-1} at ambient condition (25 °C, 50% RH), which is sufficient for the encapsulation of organic electronic devices such as OSCs.

The multilayer TFE was applied to OSC to improve the environmental stability of the device. Fig. 5(a) illustrates the *J-V* characteristics of the OSC before and after the integration of the three dyad-multilayer onto the cell. There is no obvious change in *J-V* behavior, and the PCE before and after the encapsulation was 4.60% and 4.58%, respectively. The result indicates that no noticeable degradation took place during the application of the multilayer TFE. As shown in Table S1, when Al_2O_3 was directly deposited on the cells, the average PCE decrease was about 5%. However, introducing the iCVD organic layer before the ALD process could reduce the PCE decrease. The iCVD organic layers successfully served as a temporary barrier against H_2O which is injected as the reactants in ALD process, thereby protecting the cells from degradation during the deposition. It can be confirmed that the continuous deposition of iCVD and ALD processes in this research do not damage the OSC performance, and that the encapsulation method is suitable for OSC application. Fig. 5(b) demonstrates the shelf life of OSCs encapsulated directly with the TFE developed in this study. Within the OSCs, PEPOT : PSS was deliberately chosen over MoO_x as the anodic buffer layer since PEDOT : PSS is less endurable against moisture [33,34]. Thus, with this more sensitive cell, we could visualize the effect of encapsulation more clearly. Also, a definite correlation between barrier property of TFE and the shelf life of OSCs was confirmed as shown in Fig. 5(b). Cell encapsulated with only one organic layer was degraded immediately upon exposure to the accelerated condition of 27 °C and 90% RH, just as the OSCs without encapsulation. During the degradation, both short circuit current and open circuit voltage were decreased simultaneously as shown in Table S2. Considering the WVTR value of one dyad-multilayer

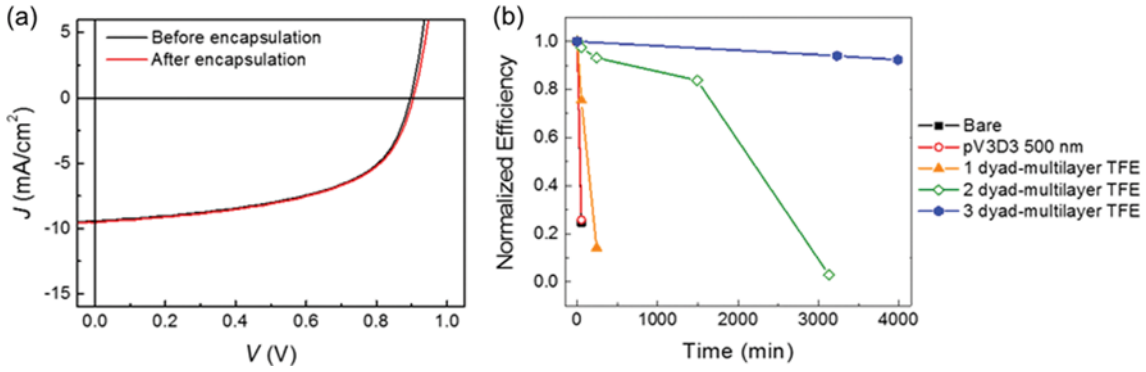

Fig. 5. (a) *J-V* characteristics of OSC before and after application of the multilayer-TFE. (b) Shelf life of OSCs encapsulated with pV3D3, and one to three dyads of pV3D3/Al_2O_3 multilayer-TFE.

TFE, the cell surprisingly degraded quickly. It can be assumed that extrinsic factors such as side penetration or particles might have accelerated the device degradation. However, with the increase of the number of multilayer dyads, the shelf life of the cells increased significantly and the cell encapsulated with three dyad-multilayer TFE retained 92.4% of initial PCE of OSCs even after the exposure of the OSC in the accelerated condition for about 4,000 min, which is fully consistent with previous observation that WVTR of at least 10^{-4} g·m^{-2}·day^{-1} is required for encapsulation of OSCs [17]. The substantial enhancement of OSC shelf life achieved by encapsulation with three dyad-multilayer TFE clearly indicates that the monolithic encapsulation of OSCs with pV3D3/Al_2O_3 multilayer TFE can be a powerful tool to increase the stability of organic electronics.

CONCLUSION

An organic/inorganic multilayer TFE with both excellent optical and barrier properties was successfully fabricated by alternative deposition of iCVD organic layer and ALD inorganic layer. pV3D3, which was introduced as a superb dielectric layer, could be stacked with Al_2O_3 film multiple times to form the high-performance multilayer TFE with smooth, defect-free interface. Moreover, the pV3D3/Al_2O_3 multilayer TFE was extremely transparent with an average transparency of 99.5% in visible light region. The WVTR at ambient condition was estimated to be as low as 1.27×10^{-5} g·m^{-2}·day^{-1}, showing that the barrier property of the TFE could meet the OSC encapsulation requirement. Finally, the developed hybrid TFE was applied monolithically to encapsulate OSCs, and greatly increased the shelf life of the cells.

ACKNOWLEDGEMENT

This work was supported by the National Research Foundation of Korea (NRF) grants funded by the Ministry of Science, ICT & Future Planning (MSIP) of Korea under Contract Number, NRF-2015M1A2A2056542 (climate change program).

SUPPORTING INFORMATION

Additional information as noted in the text. This information is available via the Internet at http://www.springer.com/chemistry/journal/11814.

REFERENCES

1. L. El Chaar, L. A. Lamont and N. El Zein, *Renew. Sust. Energy Rev.*, **15**, 2165 (2011).
2. R. García-Valverde, J. A. Cherni and A. Urbina, *Prog. Photovolt.: Res. Appl.*, **18**, 535 (2010).
3. M. Jørgensen, K. Norrman, S. A. Gevorgyan, T. Tromholt, B. Andreasen and F. C. Krebs, *Adv. Mater.*, **24**, 580 (2012).
4. J. Huang, J. H. Carpenter, C. Z. Li, J. S. Yu, H. Ade and A. K. Jen, *Adv. Mater.*, **28**, 967 (2016).
5. A. R. b. M. Yusoff, D. Kim, H. P. Kim, F. K. Shneider, W. J. da Silva and J. Jang, *Energy Environ. Sci.*, **8**, 303 (2015).
6. R. Roesch, T. Faber, E. von Hauff, T. M. Brown, M. Lira-Cantu and H. Hoppe, *Adv. Energy Mater.*, **5**, 1501407 (2015).
7. P. Cheng and X. Zhan, *Chem. Soc. Rev.*, **45**, 2544 (2016).
8. J. Ahmad, K. Bazaka, L. J. Anderson, R. D. White and M. V. Jacob, *Renew. Sust. Energy Rev.*, **27**, 104 (2013).
9. M. Manceau, E. Bundgaard, J. E. Carlé, O. Hagemann, M. Helgesen, R. Søndergaard, M. Jørgensen and F. C. Krebs, *J. Mater. Chem.*, **21**, 4132 (2011).
10. T. I. Ryu, Y. Yoon, J.-H. Kim, D.-H. Hwang, M. J. Ko, D.-K. Lee, J. Y. Kim, H. Kim, N.-G. Park, B. Kim and H. J. Son, *Macromolecules*, **47**, 6270 (2014).
11. X. Hao, S. Wang, T. Sakurai, S. Masuda and K. Akimoto, *ACS Appl. Mater. Interfaces*, **7**, 18379 (2015).
12. D. Han and S. Yoo, *Sol. Energy Mat. Sol. C*, **128**, 41 (2014).
13. D. J. Kang, H. Kang, K.-H. Kim and B. Kim, *ACS Nano*, **6**, 7902 (2012).
14. M. Wang, Q. Tang, J. An, F. Xie, J. Chen, S. Zheng, K. Y. Wong, Q. Miao and J. Xu, *ACS Appl. Mater. Interfaces*, **2**, 2699 (2010).
15. M. He, J. Jung, F. Qiu and Z. Lin, *J. Mater. Chem.*, **22**, 24254 (2012).
16. W. Wang, M. Song, T.-S. Bae, Y. H. Park, Y.-C. Kang, S.-G. Lee, S.-Y. Kim, D. H. Kim, S. Lee, G. Min, G.-H. Lee, J.-W. Kang and J. Yun, *Adv. Funct. Mater.*, **24**, 1551 (2014).
17. M. Jørgensen, K. Norrman and F. C. Krebs, *Sol. Energy Mat. Sol. C*, **92**, 686 (2008).
18. B. J. Kim, D. H. Kim, S. Y. Kang, S. D. Ahn and S. G. Im, *J. Appl. Polym. Sci.*, **131**, 40974 (2014).
19. S. Y. Kim, B. J. Kim, D. H. Kim and S. G. Im, *RSC Adv.*, **5**, 68485 (2015).
20. S. M. George, *Chem. Rev.*, **110**, 111 (2010).
21. D. A. Spee, M. R. Schipper, C. H. M. van der Werf, J. K. Rath and R. E. I. Schropp, *Thin Solid Films*, **532**, 84 (2013).
22. A. M. Coclite, G. Ozaydin-Ince, F. Palumbo, A. Milella and K. K. Gleason, *Plasma Process Polym.*, **7**, 561 (2010).
23. M. C. Barr, J. A. Rowehl, R. R. Lunt, J. Xu, A. Wang, C. M. Boyce, S. G. Im, V. Bulovic and K. K. Gleason, *Adv. Mater.*, **23**, 3499 (2011).
24. K. Pak, H. Seong, J. Choi, W. S. Hwang and S. G. Im, *Adv. Funct. Mater.* (2016), DOI:10.1002/adfm.201602585.
25. J. A. Bertrand and S. M. George, *J. Vac. Sci. Technol. A*, **31**, 01A122 (2013).
26. M. O. Reese, S. A. Gevorgyan, M. Jørgensen, E. Bundgaard, S. R. Kurtz, D. S. Ginley, D. C. Olson, M. T. Lloyd, P. Morvillo, E. A. Katz, A. Elschner, O. Haillant, T. R. Currier, V. Shrotriya, M. Hermenau, M. Riede, K. R. Kirov, G. Trimmel, T. Rath, O. Inganäs, F. Zhang, M. Andersson, K. Tvingstedt, M. Lira-Cantu, D. Laird, C. McGuiness, S. Gowrisanker, M. Pannone, M. Xiao, J. Hauch, R. Steim, D. M. DeLongchamp, R. Rösch, H. Hoppe, N. Espinosa, A. Urbina, G. Yaman-Uzunoglu, J.-B. Bonekamp, A. J. J. M. van Breemen, C. Girotto, E. Voroshazi and F. C. Krebs, *Sol. Energy Mat. Sol. C*, **95**, 1253 (2011).
27. P. F. Carcia, R. S. McLean, M. H. Reilly, M. D. Groner and S. M. George, *Appl. Phys. Lett.*, **89**, 031915 (2006).
28. H. Moon, H. Seong, W. C. Shin, W. T. Park, M. Kim, S. Lee, J. H. Bong, Y. Y. Noh, B. J. Cho, S. Yoo and S. G. Im, *Nat. Mater.*, **14**, 628 (2015).
29. J. D. Affinito, S. Eufinger, M. E. Gross, G. L. Graff and P. M. Martin, *Thin Solid Films*, **308-309**, 19 (1997).

30. S.-W. Seo, H. Chae, S. J. Seo, H. K. Chung and S. M. Cho, *Appl. Phys. Lett.*, **102**, 161908 (2013).
31. G. L. Graff, R. E. Williford and P. E. Burrows, *J. Appl. Phys.*, **96**, 1840 (2004).
32. D. J. Coyle, *Prog. Photovolt.: Res. Appl.*, **21**, 156 (2013).
33. D. Han, H. Lee, S. Jeong, J. Lee, J.-Y. Lee and S. Yoo, *Org. Electron.*, **25**, 31 (2015).
34. E. Voroshazi, B. Verreet, A. Buri, R. Müller, D. Di Nuzzo and P. Heremans, *Org. Electron.*, **12**, 736 (2011).

Supporting Information

Organic/inorganic multilayer thin film encapsulation via initiated chemical vapor deposition and atomic layer deposition for its application to organic solar cells

Bong Jun Kim*, Donggeon Han, Seunghyup Yoo**, and Sung Gap Im*,†**

*Department of Chemical & Biomolecular Engineering, Korea Advanced Institute of Science and Technology, Daejeon 34141, Korea
**Department of Electrical Engineering, Korea Advanced Institute of Science and Technology, Daejeon 34141, Korea
(*Received 13 August 2016 • accepted 24 October 2016*)

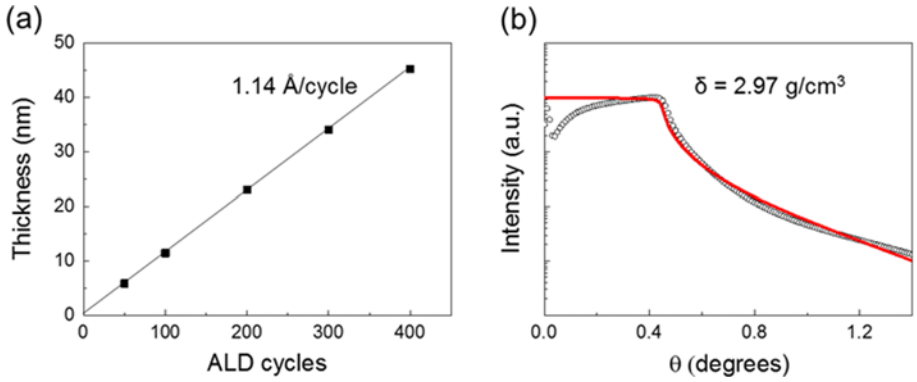

Fig. S1. (a) Growth rate of Al_2O_3 deposited by ALD in this study. (b) XRR data of 50 nm-thick Al_2O_3 deposited on Si wafer for measuring the film density.

Table S1. Representative data of OSC characteristics before and after deposition of iCVD, ALD, and three dyads of iCVD/ALD multilayer

	J_{sc}		V_{oc}		FF		PCE	
	Before	After	Before	After	Before	After	Before	After
iCVD process	−10.17	−10.11	0.924	0.922	0.56	0.57	5.30	5.31
ALD process	−10.45	−10.36	0.942	0.933	0.58	0.56	5.71	5.39
iCVD/ALD 3 dyad	−10.53	−10.57	0.899	0.904	0.49	0.48	4.60	4.58

Table S2. Representative data of OSC characteristics before and after degradation during shelf life measurement

	J_{sc}	V_{oc}	FF	PCE
Initial	−10.01	0.924	0.56	5.14
After degradation	−8.09	0.813	0.46	2.99